Available online at www.sciencedirect.com

ScienceDirect

Scripta Materialia 105 (2015) 14–17

Scripta MATERIALIA

www.elsevier.com/locate/scriptamat

On the role of thermal fluid dynamics into the evolution of porosity during selective laser melting

C. Panwisawas,* C.L. Qiu, Y. Sovani, J.W. Brooks, M.M. Attallah and H.C. Basoalto

School of Metallurgy and Materials, University of Birmingham, Edgbaston, Birmingham B15 2TT, United Kingdom

Received 6 April 2015; accepted 19 April 2015
Available online 29 April 2015

Thermal fluid dynamics and experiments have been used to study the evolution of pores during selective laser melting of Ti-6Al-4V. Scanning electron micrographs show that the morphology of pores changed from near-spherical to elongated shape as the laser scan speed increased. Computational fluid dynamics suggests that this is caused by the change of flow pattern in the melt pool which is dictated by forces such as vapour pressure, gravitational force, capillary and thermal capillary forces exerted on the metallic/gaseous interface.

Keywords: Thermal fluid dynamics; Porosity; Selective laser melting; Ti-6Al-4V

Selective laser melting (SLM) is one of the additive manufacturing (AM) processes, in which functional, complex parts are fabricated by selectively consecutive layers of powder particle using a laser beam. The technology enables a wide spectrum of possibilities to construct three-dimensional (3D) printing exclusively utilised in various technological applications [1], particularly in light-weight cellular materials [2], ranging from biomedical tissue engineering [3,4] to aerospace sector including both aeronautics and astronautics [5]. It can be seen that this novel innovation provides a high level of flexibility for processing and applications, including SLM of metallic components which have been widely reviewed elsewhere [6,7].

Nevertheless, some imperfection of parts produced by this novel manufacturing process has been observed in the SLM of aerospace materials such as nickel-based superalloys [8,9] and titanium-based alloys [10–12]. Common issues that are usually found include residual stresses and distortion [9], cracking, microstructure dependence of process conditions, and porosity [13,14]. Once one of those occurs, it is known to affect the mechanical property and subsequently the process integrity. Porosity, which is the main focus in this work, is one of the processing-induced phenomena, which is frequently found in many manufacturing processes including SLM. The propensity of porosity formation depends strongly upon the processing conditions used to produce the part.

There is still disagreement over the mechanism by which porosity forms (especially spherical pores) in SLM-fabricated samples, although it is generally believed that irregular-shaped pores are caused by lack of fusion/melting [15–17]. Thijs et al. [18] attributed the formation of spherical pores to the collapse of key holes in an aluminium alloy but suggested that in a Ti-based alloy spherical pores [13] were formed by powder denudation around the melt pool within a layer and an accumulation of the surface roughness across the layers. Vilaro et al. [19] suggested that the spherical pores were due to gas entrapment during melting and rapid solidification. Qiu et al. [14] directly observed open pores on the top surfaces of samples and argued that the spherical pores could be due to incomplete re-melting of some localised sites on the previous layer and to the insufficient feeding of molten metal to these sites.

To the best of authors' knowledge, little has been reported about the fundamental, physical effects of the fluid flow and heat transfer of the melt material which is a main driving mechanism for morphological development of porosity in these circumstances and an unequivocal explanation for porosity evolution during SLM in titanium alloys is unavailable. The overarching goal of this paper is to provide fundamental insights into the morphological development of porosity in SLM via a computational thermal fluid dynamics calculation, backed up by targeted experimentation. However, the rationalisation of porosity formation mechanism is to be published elsewhere.

In this work, a series of SLM experiments have been performed to investigate the influence of laser scanning speed on the morphology of porosity. A Concept Laser M2 Cusing SLM system, which employs an Nd:YAG laser with a wavelength of 1075 nm and a constant beam spot size of 50 μm in diameter, was used to build cubic samples with a dimension of 10 mm × 10 mm × 10 mm at a constant laser power of 400 W but with laser scanning speed ranging from 2000 mm/s to 4200 mm/s. Gas atomised Ti-6Al-4V powder

* Corresponding author; e-mail: c.panwisawas@bham.ac.uk

http://dx.doi.org/10.1016/j.scriptamat.2015.04.016
1359-6462/

with a size range of 20–50 μm supplied by TLS Technik GmbH was used and a layer thickness of 20 μm was applied during building. Metallographic samples were prepared and characterised by scanning electron microscopy (SEM) using a JEOL 7000 FEG-SEM microscope.

To better understand the morphological evolution of porosity during SLM, a mathematical modelling of thermal fluid dynamics is established in open-source code so-called Open Field Operation and Manipulation (OpenFOAM®). The physics-based model concerns about the liquid–gas interaction of the laser heat source and the material giving rise to liquid–gas interface evolution. Finite volume method is employed to take into account the effect by solving a set of conservation equations. The calculation was performed on a domain of dimension 2000 μm × 250 μm × 350 μm on a fixed mesh size of 5 μm containing 1,600,000 elements, on which a closed-packed layer of 2 row powder particles of the size 50 μm with ∼100 μm layer thickness were made to sit on the 2000 μm × 250 μm × 50 μm rectangular plate. Gaussian's surface heat source has been scanned and described by prescribed scanning speed and laser power.

In computational fluid dynamics (CFD), the sum of metallic α_1 and gaseous α_2 phase fractions is always unity, $\alpha_1 + \alpha_2 = 1$, and the weight function of any parameter x, defined as $\bar{x} = x_1\alpha_1 + x_2\alpha_2$, is used to smear out the effect of metallic and gaseous phases. To rationalise the melt dynamics, a fluid flow and heat transfer needed to be solved by assuming that the liquid Ti-6Al-4V is incompressible so that the continuity condition is written as $\vec{\nabla} \cdot \vec{u} = 0$; here $\vec{u}$ is flow velocity. Use is made of volume-of-fluid equation to compute the liquid–gas interface using $\frac{\partial \alpha_1}{\partial t} + \vec{\nabla} \cdot (\alpha_1 \vec{u}) = -\frac{\dot{m}_V}{\rho_2}$, where t is time. Evaporation occurs in the fashion that evaporation temperature T_V is reached; here mass evaporation rate $\dot{m}_V = p_V\sqrt{\frac{m}{2\pi k_B T}}$ and gas density ρ_2, which is assumed to be the same as metallic vapour density, is defined. No chemical concentration has been considered in this work. Here, recoil pressure as a function of temperature T is defined by $p_V(T) = p_0 \exp\left\{\frac{\Delta H_V}{R}\left(\frac{1}{T_V} - \frac{1}{T}\right)\right\}$, where atmospheric pressure p_0, enthalpy change of evaporation ΔH_V, and gas constant R are used. To calculate the thermal fluid dynamics of the melt pool during the SLM, the full couple equations of the Navier–Stokes equation,

$$\frac{\partial \bar{\rho}\vec{u}}{\partial t} + \vec{\nabla} \cdot (\bar{\rho}\vec{u} \otimes \vec{u}) = -\vec{\nabla}p + \vec{\nabla} \cdot \bar{\bar{T}} + \bar{\rho}g\hat{e}_z\beta(T - T_{ref}) - K_C\left(\frac{(1-f_L)^2}{f_L^3 + C_K}\right)\vec{u} + \left[\sigma\kappa\hat{n} + \frac{d\sigma}{dT}(\vec{\nabla}T - \hat{n}(\hat{n}\cdot\vec{\nabla}T)) + p_V\right] |\vec{\nabla}\alpha_1| \frac{2\bar{\rho}}{(\rho_1 + \rho_2)} \quad (1)$$

the conservation of thermal energy,

$$\frac{\partial \bar{\rho}\bar{C}_pT}{\partial t} + \vec{\nabla} \cdot (\bar{\rho}\vec{u}\bar{C}_pT) = -\frac{\partial \bar{\rho}\Delta H_f}{\partial t} - \vec{\nabla} \cdot (\bar{\rho}\vec{u}\Delta H_f) + \vec{\nabla} \cdot (\bar{k}\vec{\nabla}T) - \left[(\sigma_s\epsilon(T^4 - T_{ref}^4) + Q_V)|\vec{\nabla}\alpha_1| - Q_T\right] \frac{2\bar{\rho}\bar{C}_p}{\left(\rho_1 C_{p1} + \rho_{2C_{p2}}\right)} \quad (2)$$

the continuity equation and the volume-of-fluid equation are solved to quantify the melt flow dynamics. Eq. (1) indicates that the rate of change of the momentum of fluid on RHS is driven by the summation of all inter-facial forces interacting in the system. Divergence of stresses is written in two parts, first two terms of LHS of Eq. (1), in terms of pressure p(hydrostatic stress tensor) and deviatoric stress tensor $\bar{\bar{T}} = 2\bar{\mu}\left[\left(\frac{1}{2}\vec{\nabla}\vec{u} + \frac{1}{2}(\vec{\nabla}\vec{u})^T\right) - \frac{1}{3}\left(\vec{\nabla}\cdot\vec{u}\right)II\right]$. Other body forces considered in this work are (i) buoyancy force caused by density differences in the liquid metal pool due to thermal expansion β, (ii) melting force via Darcy's term written as a function of liquid volume fraction f_L where $f_L = \frac{1}{2}\mathrm{erf}\left(\frac{T - T_m}{T_L - T_S}\right) + \frac{1}{2}$ when T_s, T_L and T_m solidus temperature, liquidus temperature and arithmetic mean between T_s and T_L, and (iii) surface force terms due to capillary, Marangoni's force and recoil pressure applied on the liquid–gas interface $|\vec{\nabla}\alpha_1|$ and shaper surface factor $\frac{2\bar{\rho}}{(\rho_1+\rho_2)}$ and $\frac{2\bar{\rho}\bar{C}_p}{(\rho_1 C_{p1} + \rho_{2C_{p2}})}$ used to smear out the effect of very different density phases. Capillary force acts on curvature κ at normal direction $\hat{n}$ with the surface tension σ, whereas Marangoni force, caused by $\frac{d\sigma}{dT}$ and $\vec{\nabla}T$, is fully integrated in this model. As for the balance of thermal energy in Eq. (2), the heat input due to the laser heat source term Q_T, adopted from [20], leads to heat loss due to conduction defined by thermal conduction coefficient $\bar{k}$, radiation using Stefan–Boltzmann constant σ_s and emissivity ε to calculate the heat loss, evaporation $Q_V \sim \dot{m}_V\Delta H_V$, and energy dissipation during melting in which enthalpy change of melting ΔH_f has been considered. All of these have been simulated to describe the liquid–gas interface and formulate the fundamental insights into melt pool dynamics leading to morphological evolution of porosity. Model parameters of Ti-6Al-4V were adopted from Refs. [21–23].

Figure 1 shows the variation of porosity level as a function of laser scanning speed at a fixed laser power (400 W). It can be seen that the samples fabricated below 2500 mm/s generally show lower porosity level than those fabricated above this speed. Moreover, it is noted that the samples fabricated below 2500 mm/s contain so-called intra-layer pores with spherical, elliptical or triangular morphologies (see Fig. 2(a–c)) whereas the samples fabricated above 3000 mm/s tend to be dominated by horizontal elongated

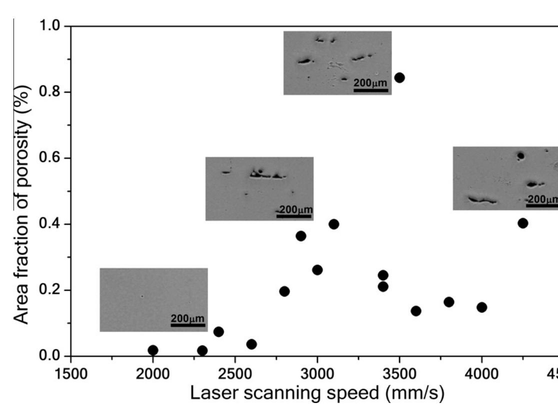

Figure 1. Variation of area fraction of porosity with laser scanning speed by using constant laser power.